scientific reports

Check for updates

OPEN

Lamc1 promotes osteogenic differentiation and inhibits adipogenic differentiation of bone marrow-derived mesenchymal stem cells

Lixia Zhao[1,2], Shuai Liu[1,2], Yanqiu Peng[1] & Jian Zhang[1]✉

Bone marrow-derived mesenchymal stem cells (BMSCs) exhibit multi-lineage differentiation potential and robust proliferative capacity. The late stage of differentiation signifies the functional maturation and characterization of specific cell lineages, which is crucial for studying lineage-specific differentiation mechanisms. However, the molecular processes governing late-stage BMSC differentiation remain poorly understood. This study aimed to elucidate the key biological processes involved in late-stage BMSC differentiation. Publicly available transcriptomic data from human BMSCs were analyzed after approximately 14 days of osteogenic, adipogenic, and chondrogenic differentiation. Thirty-one differentially expressed genes (DEGs) associated with differentiation were identified. Pathway enrichment analysis indicated that the DEGs were involved in extracellular matrix (ECM)-receptor interactions, focal adhesion, and glycolipid biosynthesis, a ganglion series process. Subsequently, the target genes were validated using publicly available single-cell RNA-seq data from mouse BMSCs. Lamc1 exhibited predominant distribution in adipocytes and osteoblasts, primarily during the G2/M phase. Tln2 and Hexb were expressed in chondroblasts, osteoblasts, and adipocytes, while St3gal5 was abundantly distributed in stem cells. Cell communication analysis identified two receptors that interact with LAMCI. q-PCR results confirmed the upregulation of Lamc1, Tln2, Hexb, and St3gal5 during osteogenic differentiation and their downregulation during adipogenic differentiation. Knockdown of Lamc1 inhibited adipogenic and osteogenic differentiation. In conclusion, this study identified four genes, Lamc1, Tln2, Hexb, and St3gal5, that may play important roles in the late-stage differentiation of BMSCs. It elucidated their interactions and the pathways they influence, providing a foundation for further research on BMSC differentiation.

Keywords Mesenchymal stem cell, Osteogenesis, Adipogenesis, Laminin, Single-cell RNA-seq

Mesenchymal stem cells (MSCs) are pluripotent that can be obtained from various tissues, umbilical cord, amniotic fluid, and placenta[1–4]. It is capable of expanding and differentiating in vitro into a variety of mesodermal-type lineages, including bone, adipose, cartilage, muscle, tendon, and stroma, supporting hematopoiesis and the vascular system, and undergoes migration and paracrine signaling, which is not only crucial in embryonic development but also plays an important role in tissue homeostasis and repair throughout the life of an organism[5,6]. MSCs from different sources exhibit different differentiation tendencies, and studies have shown that BMSCs exhibit greater APL activity, calcium deposition, and transformation capacity at an earlier age,compared with adipose-derived MSCs[7]. Therefore, BMSCs were chosen for studying the molecular mechanisms of osteogenic differentiation.

Key transcription factors for osteoblast differentiation are required for the expression of osteoblast-specific genes, including Runt-associated transcription factor 2 (Runx2) and osteocalcin (Ocn), alkaline phosphatase (ALP), type I collagen, bone bridging proteins, and bone sialic acid protein[8–13]. Bone morphogenetic proteins (BMPs), especially BMP-2, BMP-4, and BMP-7, activate the Smad signaling pathway, which in turn leads to the expression of Runx2 and Ocn and inhibits adipogenic differentiation[14–16]. In addition to BMP, the Wnt/β-catenin signaling pathway plays a key role in osteoblast differentiation[17]. Activation of this pathway leads to the

[1]Bioengineering College, Zunyi Medical University, 368 Jinwan Road, Zhuhai 519090, Guangdong, China. [2]These authors contributed equally: Lixia Zhao and Shuai Liu. ✉email: jianzhang@zmu.edu.cn

accumulation of β-catenin in the cytoplasm, which then translocates to the nucleus, activates the transcription of osteoblast-specific genes, and inhibits adipogenesis. On the other hand, adipocyte differentiation is regulated by peroxisome proliferator-activated receptor γ (PPARγ)[18]. PPARγ is considered a major regulator of adipogenesis because it controls the expression of many adipocyte-specific genes. PPARγ activation not only promotes adipogenesis but also inhibits osteogenesis[19]. The balance between osteoblast and adipocyte differentiation is a tightly regulated process[20]. Therefore, understanding the mechanisms that regulate this balance is essential for developing therapeutic approaches for diseases such as osteoporosis and obesity, which are characterized by an imbalance between bone and fat formation.

In mesenchymal stem cells, cellular matrix components play a key regulatory role in the directed differentiation of mesoderm into osteoblasts or adipogenic cells[21]. The extracellular matrix is a complex network of many molecules, including collagens, glycoproteins (GPs), and ECM-associated proteins[22]. Specific components of the ECM can influence cell fate decisions; for instance, collagen promotes osteoblast differentiation, whereas fibronectin may promote adipogenic cell differentiation[23,24]. Cell adhesion molecules and cell signaling molecules in the cell matrix are important regulators of the differentiation process, transmitting signals and modulating cell behavior by interacting with receptors on the cell surface[25,26]. For example, integrins increase the ability of cells to differentiate osteoblastically, maintain bone homeostasis, and regulate bone mass while inhibiting the adipogenic differentiation of BMSCs[27–29]. Taken together, the study of cellular matrix components contributes to our understanding of the mechanisms of germ layer-directed differentiation.

BMSCs exhibit the most pronounced difference between days 14 and 17 of differentiation, and the difference between days 17 and 21 of differentiation is not significant[7]. Therefore, our study combined tri-lineage differentiation with bulk RNA-seq analysis and single-cell RNA-seq (scRNA-seq) analysis to determine which factors simultaneously play key roles in osteogenic, adipogenic, and chondrogenic terminal phase differentiation, and cell staining and RT-qPCR were used to verify the changes in target genes during differentiation, aiming to provide a new basis for MSC therapies.

Results

hBMSCs osteogenic, adipogenic, and chondrogenic differentiation 14-day transcriptome data cross-identify 31 DEGs

A preliminary comparison of the six datasets (GSE36923, GSE44303, GSE109503, GSE140861, GSE28205, GSE37558) was performed before the differential gene analysis. Through the box-and-line plot of the distribution of the 6 datasets, we concluded that there was no batch effect within the datasets (Fig. 1a–c). According to the PCA plot of the distribution of the 6 datasets, the differences between different types of data were significant, and the analysis was feasible (Fig. 1d–i). Differential gene analysis of different types of data was performed separately, and DEGs coexpressed in similar datasets were selected to obtain 347 upregulated genes and 263 downregulated genes related to osteogenic differentiation, 658 upregulated genes and 704 downregulated genes related to adipogenic differentiation, and 106 upregulated genes and 48 downregulated genes related to cartilaginous differentiation (Fig. 2a–i). There was an antagonistic relationship between the three classifications. To identify the genes that were coexpressed in each category based on the Venn diagram, the genes coexpressed in osteogenic, adipogenic, and chondrogenic differentiation were compared two by two with opposite differentiation trends, and a total of 31 DEGs were obtained (Fig. 2j–o).

Enrichment analysis revealed that DEGs were concentrated in the extracellular matrix and related to ECM-receptor interactions

Gene Ontology (GO) analysis revealed that the differentially expressed genes (DEGs) associated with an adjusted p-value (adj. P) < 0.05 were primarily enriched in biological processes and molecular functions related to collagen-containing extracellular matrix, hexosaminidase activity, binding to laminin, structural components of the extracellular matrix that confer tensile strength, and integrin binding (Fig. 2p). At KEGG pathway analysis revealed that DEGs with adj.P < 0.05 were associated with the ECM-receptor interaction, local adhesion, and glycolipid biosynthesis-ganglio series pathways (Fig. 2q).

ceRNA network construction

Using the String website, six target genes enriched in extracellular mesenchymal tissues were identified, namely, Hapln1, Col4a1, Lamc1, Itga10, Col10a14, and Tln2, and two genes enriched in the target genes involved in the biosynthesis of glycosphingolipid-ganglio series pathways were identified, namely, Hexb and St3gal5 (Fig. 3a,b). The gene symbols, abbreviations and functions are shown in Table 1. The two PPI networks of the target genes (60 nodes, 115 edges; 19 nodes, 20 edges) were obtained through the MCODE module of Cytoscape, with retention greater than or equal to 2, K-Core taken as 2, and Max. depth taken as 100 nodes. mRNAs are pink, miRNAs are purple, and lncRNAs are orange; the greater the connectivity of the nodes is, the greater the number of nodes. Lamc1 and Col4a1 are the core of the mRNA-miRNA-lncRNA interaction network and are closely related to noncoding RNAs that have been shown to play important roles in osteogenesis or adipogenesis, such as MALAT1, H19, XIST, and NEAT1.

Target gene expression was higher at both the adipose gene level and tissue level than at bone tissue

Analysis of the Human Protein Atlas (HPA) database revealed that the expression levels of Col4a1 and Lamc1 were significantly higher in adipose tissue compared to bone marrow tissue, both at the gene and tissue levels. Similarly, Tln2 exhibited slightly elevated gene expression in adipose tissue relative to bone marrow (Fig. 3c,d). Interestingly, while Hexb and St3gal5 displayed moderately higher gene expression in adipose tissue than in

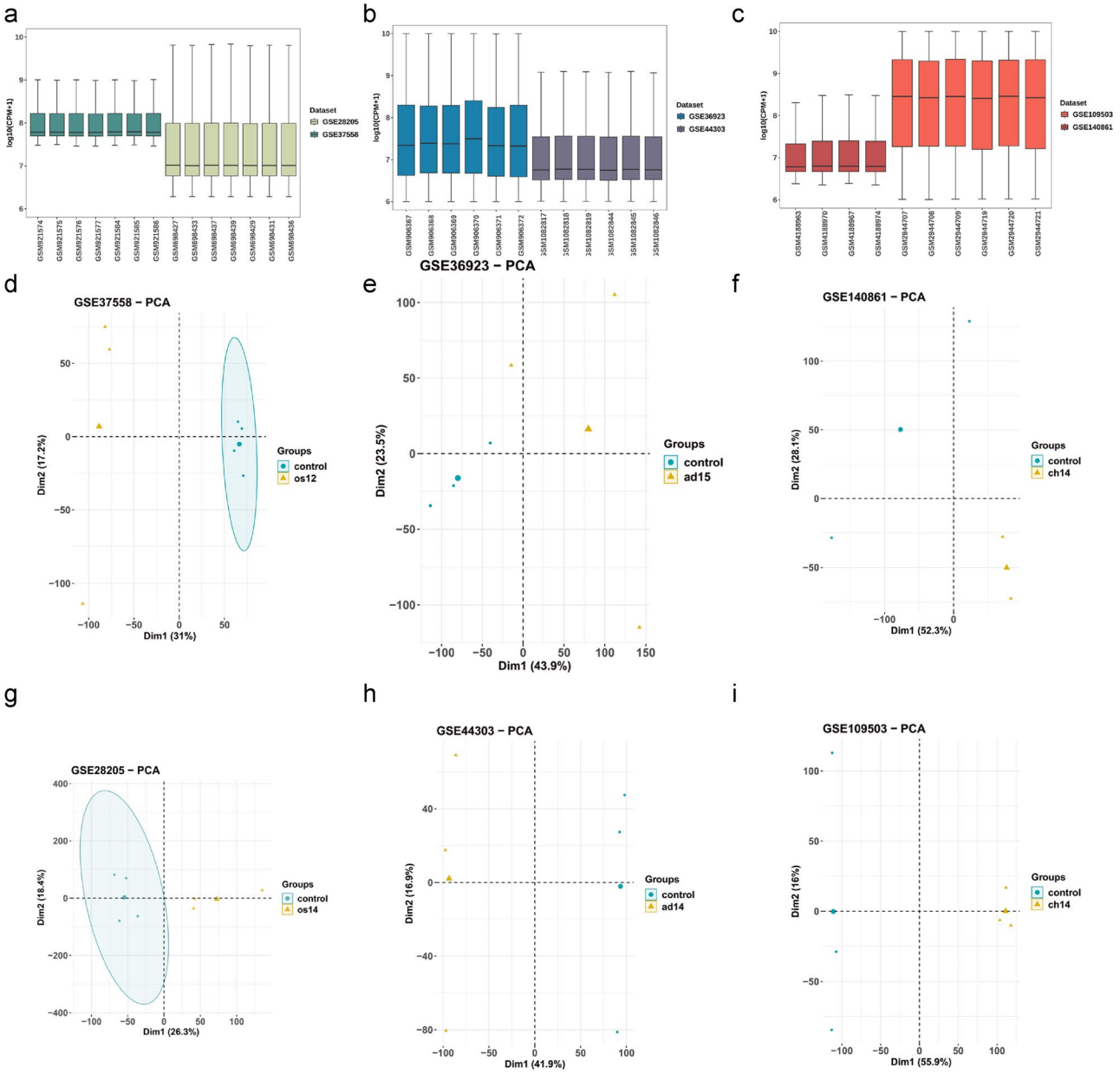

Figure 1. Quality of RNA-seq data of bone marrow-derived MSCs at the late stage of differentiation. Box plot: (**a**) osteogenic differentiation dataset (GSE28205, GSE37558); (**b**) adipogenic differentiation dataset (GSE36923, GSE44303); (**c**) chondrogenic differentiation dataset (GSE109503, GSE140861); PCA plot; (**d**) GSE37558; (**e**) GSE36923; (**f**) GSE140861; (**g**) GSE28205; (**h**) GSE44303; (**i**) GSE109503.

bone marrow, their tissue-level expression patterns were reversed, with higher levels observed in bone marrow compared to adipose tissue. The gene expression scores of the hub genes in abdominal adipose tissue, omental fat pads, subcutaneous adipose tissue, synovial joints, cartilage tissue, trabecular bone tissue, tibia, bone marrow, and myeloid cells were compared using the data obtained from the BGEE database. Col4a1 and Lamc1 had the highest expression in abdominal adipose tissue, omental fat pads, and subcutaneous adipose tissue, and Hexb had the highest expression in synovial joints, trabecular bone tissues, and bone marrow cells. Hapln1 was most highly expressed in cartilage tissues, and only Tln2 and Itga10 were expressed in bone marrow (Fig. 3e).

BMSCs are categorized into 11 clusters at single-cell resolution

We used t-distributed stochastic neighbor embedding (tSNE) to investigate cellular heterogeneity within clusters, and after the integration of the two datasets (GSE128423, GSE156635) (n = 44053), we identified 21 cell clusters and 11 cell types-osteoblasts (n = 2411), chondrocytes (n = 8251), adipogenic cells (n = 5396), endothelial cells (n = 7682), fibroblasts (n= 6949), neutrophils (n = 912), lymphocytes (n = 3957), megakaryocytes (n= 682), erythroblasts (n= 735), stem cells (n = 4908) and blastocytes (n = 2170) -and the biomarker expression of each

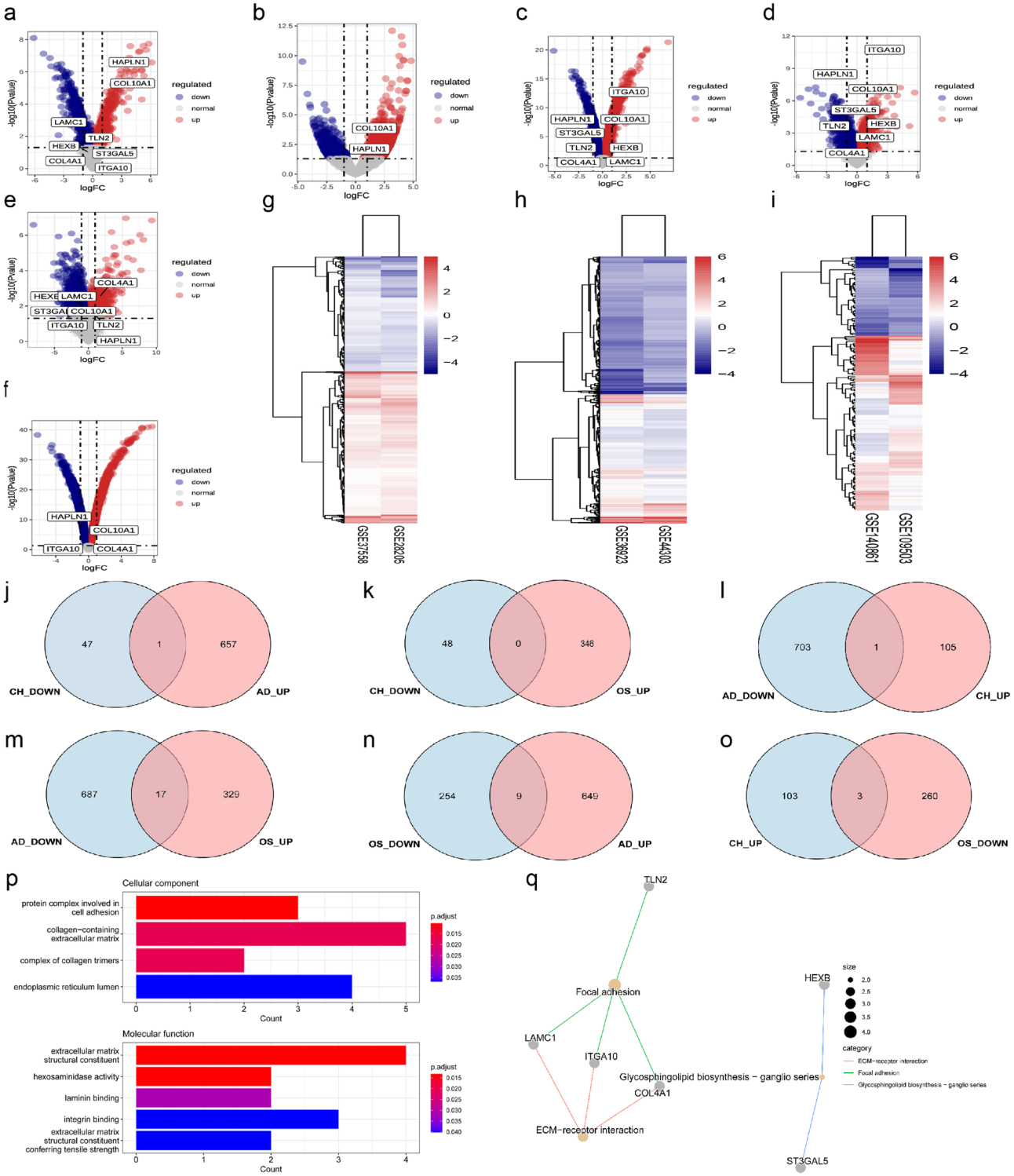

subgroup is given (Fig. 4a,b). Erythrocytes were not removed since our focus was on the directed differentiation of stem cells to adipocytes, osteoblasts, and chondrocytes. The distribution of the target genes is shown in Fig. 4c.

Scoring of scRNA-seq annotation reliability proves cluster annotation reliability

We chose three methods to evaluate the reliability of the single-cell annotations. First, we used the WNT pathway and the ADIPOGENESIS pathway to sort the cells (Fig. 5a,b). The WNT pathway was mainly distributed in osteoblasts, adipocytes, stromal cells, and chondroblasts, and the ADIPOGENESIS pathway was mainly distributed in adipocytes, stromal cells, and megakaryocytes, which was in line with our biological a priori experience. Then using the local similarity between cells, the stemness and differentiation potential of cells were assessed according to CytoTrace, and the degree of differentiation was in the following order: stem cells < chondrocytes

◂**Figure 2.** Target gene identification and enrichment analysis of RNA-seq data from bone marrow-derived MSCs at the late stage of differentiation (**a,b**) volcano plots of differential gene expression in osteogenic differentiation datasets (GSE28205 and GSE37558); (**c,d**) volcano plots of differential gene expression in adipogenic differentiation datasets (GSE36923 and GSE44303); (**e,f**) volcano plots of differential gene expression in cartilageogenic differentiation datasets (GSE109503 and GSE140861) volcano plots of differential gene expression; (**g**) heatmap of differential gene expression of osteogenic differentiation datasets (GSE28205 and GSE37558) after integration by the RRA algorithm; (**h**) heatmap of differential gene expression of adipogenic differentiation datasets (GSE36923 and GSE44303) after integration of by the RRA algorithm; (**i**) heatmap of differential gene expression of chondrogenic differentiation dataset (GSE109503 and GSE140861) heatmap of differential gene expression after integration by the RRA algorithm. Venn diagrams of DEGs with opposite differentiation trends in the three differentiation directions. A total of 31 DEGs were obtained. (**j**) Intersection of osteogenic upregulated differential genes and adipogenic downregulated differential genes; (**k**) intersection of osteogenic upregulated differential genes and chondrogenic downregulated differential genes; (**l**) intersection of chondrogenic upregulated differential genes and adipogenic downregulated differential genes; (**m**) intersection of adipogenic upregulated differential genes and chondrogenic downregulated differential genes; (**n**) intersection of adipogenic upregulated differential genes and chondrogenic downregulated differential genes; (**o**) intersection of adipogenic upregulated differential genes and osteogenic downregulated differential genes; (**p**) differential gene enrichment analysis (GO) bar graph; (**q**) differential gene enrichment analysis (KEGG) network graph. *AD* adipogenesis, *OS* osteogenesis, *CH* chondrogenesis.

< osteoblasts < adipoblasts. Col4a1 and Lamc1 were mainly distributed in adipocytes and osteoblasts; Tln2 and Hexb were expressed in chondrocytes, osteoblasts, and adipocytes; Col10a1 was distributed in a small number of chondrocytes, Itga10 and Hapln1 were distributed in a large number of chondrocytes, and St3gal5 was distributed in a large number of stem cells (Fig. 5c). Using Monocle2 to perform a time-matching analysis of the four types of cells, it was concluded that the BMSCs can be divided into two different types of sources, both of which can be differentiated into chondroblasts, and that the later stage is accompanied by the differentiation of the adipoblasts with the osteoblasts with a large number of adipoblasts (Fig. 5d). Finally, cell cycle maps for all the subpopulations were generated and we concluded that stem cells, lymphocytes, and neutrophils were in the early stage of differentiation, while the remaining subpopulations were in the late stage of differentiation (Fig. 5e).

Cell cycle analysis of target genes

Based on the scatter plots, Col4a1, Lamc1, Hapln1, Itga10, Tln2, Hexb, were expressed at all times in osteoblasts, Col10a1 and St3gal5 were expressed to a lesser extent, and Itga10 with Lamc1 became more abundantly expressed at mitotic phase (M). Scatter plots of Runx2 and Bglap expression cycles are given as reference (Fig. 6). In adipocytes, Col4a1 and Lamc1 were significantly more expressed than in osteoblasts, being abundantly expressed during mitosis (M), and Itga10, St3gal5, and Col10a1 were expressed during DNA synthesis (S), which is consistent with our previous prediction. Scatter plots of Pparγ and Fabp4 are given as reference (Fig. 7). In chondrocytes, Hapln1 and Itga10 expression is reduced and Tln2 expression is elevated in mitosis (M). Scatter plots of Sox9 and Col2a1 are given as reference (Fig. 8).

Intercellular interactions in adipogenic, osteogenic differentiation target two pairs of ligands that interact with Lamc1

In BMSCs, osteoblasts communicate with adipogenic cells when adipogenic cells are used as receptors, and all three types of cells communicate with stem cells when stem cells are used as receptors (Fig. 9a). Considering that the pathway enriched for target genes is the ECM-receptor interaction pathway, to determine the mechanism of interactions in the stroma, we investigated the most significant ligand–receptor interactions in the LAMININ pathway (Fig. 9b). Lamc1-CD44 and Lamc1-Dag1 exhibited extreme differentiation, followed by interactions at the level of individual ligands, and the ligands that interact with Lamc1 were identified. LAMC1-CD44 interaction may affect stem cell differentiation to bone or cartilage and adipose, and LAMC1-DAG1 interaction may affect osteogenic, adipogenic, and chondrogenic differentiation relationships (Fig. 9c–e).

Target genes promote osteogenic differentiation and inhibit adipogenic differentiation

The target genes Col10a1 and Hapln are predicted to play important roles in chondrogenic differentiation, and we have confirmed this in past reports. Similarly, Col4a1 and Itga10 have been shown to play important roles in osteogenic differentiation, and therefore, no subsequent validation will be performed. During osteogenic differentiation, the alizarin red staining results revealed gradual reddening with increasing days of induction, with MC3T3-E1 cells reaching the reddest at 7 days (Fig. 10a,b). We detected the expression of target genes and marker genes at 3 days, 5 days, and 7 days. Lamc1, Tln2, Hexb, and St3gal5 tended to be upregulated, and the expression of the marker gene Runx2 gradually increased to a maximum at 7 days (Fig. 10c–e). During adipogenic differentiation, as the duration of induction increased, the red intensity of the 3T3-L1 cells gradually decreased, and on day 8, the red intensity of the 3T3-L1 cells decreased (Fig. 10f,g). We detected the expression of target genes and marker genes after 4 days, 6 days, and 8 days. Lamc1, Tln2, Hexb, and St3gal5 tended to be downregulated, and the expression of the marker gene Pparγ gradually increased to a maximum on 8 days (Fig. 10h–j). Laminin can increase the expression of calcium and increase the concentration of osteocalcin. After Lamc1 was knocked down in MC3T3-E1 and 3T3-L1 cells, the gene expression levels of Runx2 and Ocn were significantly downregulated, and those of Pparγ and Fabp4 were also downregulated (Fig. 11c–e,h–j).Similarly,

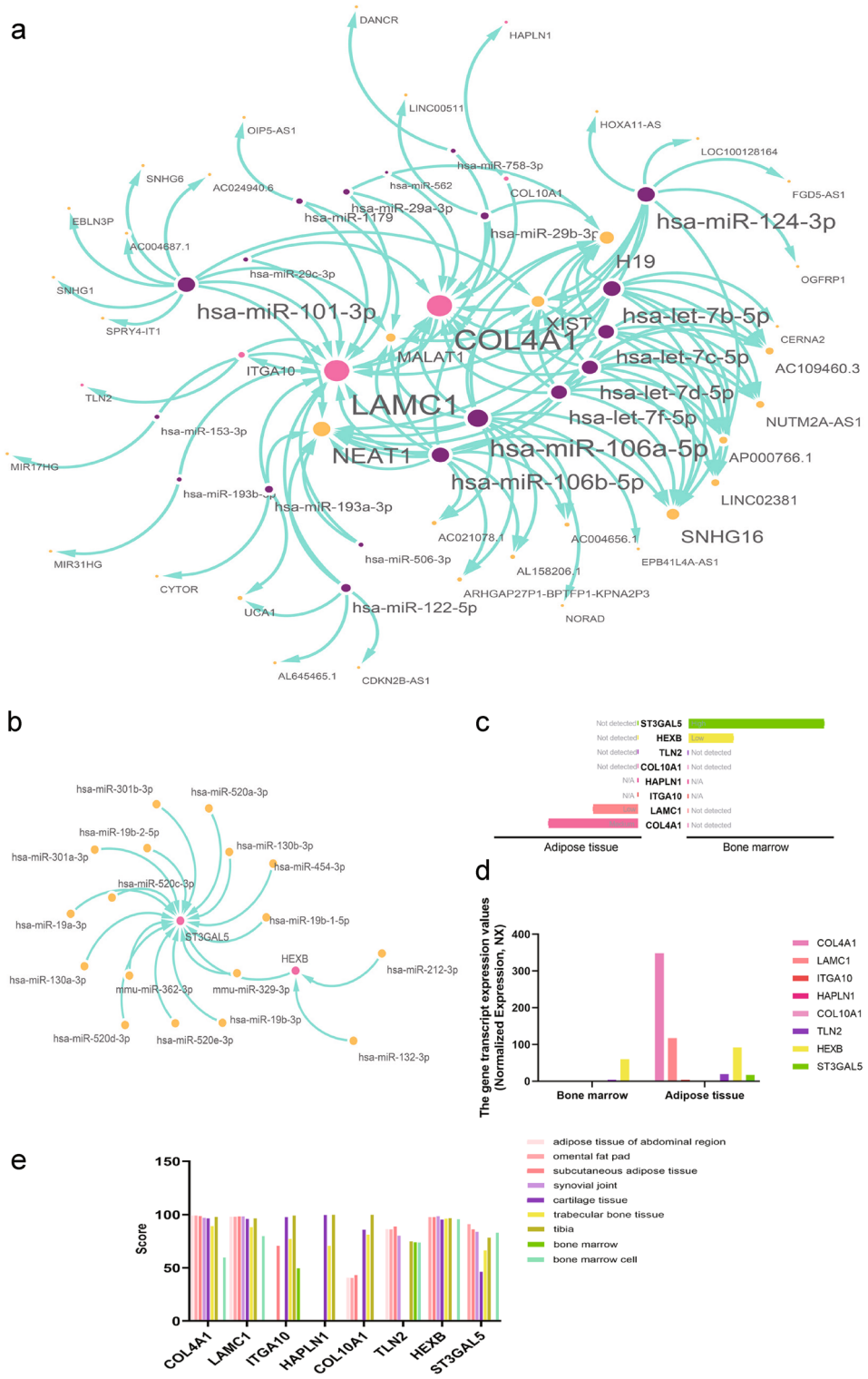

Figure 3. Expression of target genes in the database (**a**) mRNA–miRNA–lncRNA interaction network map composed of Hapln1, Col4a1, Lamc1, Itga10, Col10a1, and Tln2; (**b**) mRNA–miRNA–lncRNA interaction network map composed of Hexb and St3gal5. Expression in the HPA database; (**c**) histogram of differential gene tissue expression levels; (**d**) histogram of differential gene gene expression levels; expression in the Bgee database; (**e**) histogram of differential gene tissue expression levels.

Gene symbol	Describe	Function
Col4a1	Collagen Type IV Alpha 1 Chain	Type IV collagen proteins are integral components of basement membranes
Lamc1	Laminin Subunit Gamma 1	Laminins, a family of extracellular matrix glycoproteins, are the major noncollagenous constituent of basement membranes. They have been implicated in a wide variety of biological processes including cell adhesion, differentiation, migration, signaling, neurite outgrowth, and metastasis
Itga10	Integrin Alpha-10	They participate in cell adhesion as well as cell-surface-mediated signaling
Hapln1	Hyaluronan And Proteoglycan Link Protein 1	It is predicted to enable hyaluronic acid binding activity, to be an extracellular matrix structural constituent conferring compression resistance. And it is predicted to be involved in skeletal system development
Col10a1	Collagen Type X Alpha 1 Chain	This gene is a short chain collagen expressed by hypertrophic chondrocytes during endochondral ossification
Tln2	Talin 2	It is thought to associate with unique transmembrane receptors to form novel linkages between extracellular matrices and the actin cytoskeleton
Hexb	Hexosaminidase Subunit Beta	Related to hydrolase activity
St3gal5	ST3 Beta-Galactoside AlphA-2,3-Sialyltransferase 5	The protein encoded by this gene is a type II membrane protein

Table 1. Eight hub genes and their functions.

the red color of the knocked-down cells was significantly lighter than that of the controls (Fig. 11a,b,f,g). Similarly, the previous experiment was repeated with the housekeeping gene GAPDH and yielded similar results (Supplementary Fig. S1).

Methods

Data collection and processing

Gene expression profiling data (GSE36923, GSE44303, GSE109503, GSE140861, GSE28205 and GSE37558) were obtained from the Gene Expression Omnibus (GEO). GSE109503 contained RNA-seq data, and the remaining five gene sets were obtained from bulk RNA-seq data. GSE109503 and GSE140861 are chondrogenic differentiation datasets; GSE109503 has four subsets (two controls and two experimental groups); GSE140861 has six subsets (three controls and three experimental groups); GSE28205 and GSE37558 are osteogenic differentiation datasets; GSE28205 has six subsets (three control groups and three experimental groups); GSE37558 has six subsets (three control groups and three experimental groups); GSE36923 and GSE44303 are adipogenic differentiation datasets; GSE36923 has seven subsets (four control groups and three experimental groups); and GSE44303 has seven subsets (four controls and three experimental groups).

Single-cell RNA-seq data (GSE128423 and GSE156635) were obtained from the Gene Expression Omnibus (GEO) based on a 10× Genomics assay with eight normal BMSC tissue samples. The summary results of the gene expression profiling dataset information are provided in Table 2.

Microarray data were normalized ,and variance was analyzed using the Limma package in the R/Bioconductor software for matrix data from each GEO dataset, and RNA-seq data were normalized ,as was variance analyzed using the edgeR package. DEGs of the same cell type identified from each of the six datasets were integrated based on different differentiation categories using the RobustRankAggreg package. $|\log2FC| \geq 1$ and $P \leq 0.05$ were considered to indicate statistical significance.

PCA plots for each dataset were plotted using the FactoMineR package and the factoextra package in the R/Bioconductor software. pheatmap package was used to plot heat maps of the genes after data merging. ggplot2 package was used to plot volcano plots after data merging. Venn plots were generated using TBtools software (version x64 v1.09876). GO function enrichment and KEGG pathway enrichment were performed for 31 differential genes (DEGs) using the clusterProfiler package in R software. adj. $P \leq 0.05$ was considered statistically significant. Bar and bubble plots were drawn using the ggplot2 package, and network plots were drawn using the enrichplot package.

scRNA-seq data were preprocessed using the Seurat package in R software for matrix data from each GEO dataset, the PercentageFeatureset function was used to determine the proportion of mitochondrial genes, and correlation analyses were used to investigate the relationships between sequencing depth and mitochondrial gene sequences and total intracellular sequences. Each gene was expressed in at least 3 cells. The gene expression in each cell was greater than 500 and less than 6000, the mitochondrial content was less than 30%, and the UMI in each cell was at least greater than 200. The scRNA-seq data were normalized by the NormalizeData method after data filtering, and highly variable genes were identified by the FindVariableFeatures method to compute the mean expression and dispersion and converted to logarithmic format. Next, the data from the two scRNA-seq datasets were integrated using the Harmony package, and then we performed principal component analysis (PCA) and reduced the data to the first 17 PCA components (the number of components selected based on the standard deviation of the principal components—in the platform area of the Elbow Graph). To visualize the data, we used the Seurat package for t-distribution random neighbor embedding (tSNE) to project the cells in two-dimensional space. We visualized clusters on 2D maps generated using t-distributed random neighbor embedding (t-SNE). Clusters were annotated according to CellMarker 2.0 (http://yikedaxue.slwshop.cn/), and the annotated clusters were scored using the AUCell package, selecting the WNT pathway-a key pathway for osteogenesis- and the ADIPOGENESIS pathway-a key pathway for adipogenesis. The cell cycle of the annotated clusters was inferred using the tricycle package, and the cell cycle in which the target genes are located was determined. The Cytotrace package was used to determine the stemness and differentiation potential of stem cells, chondrocytes,

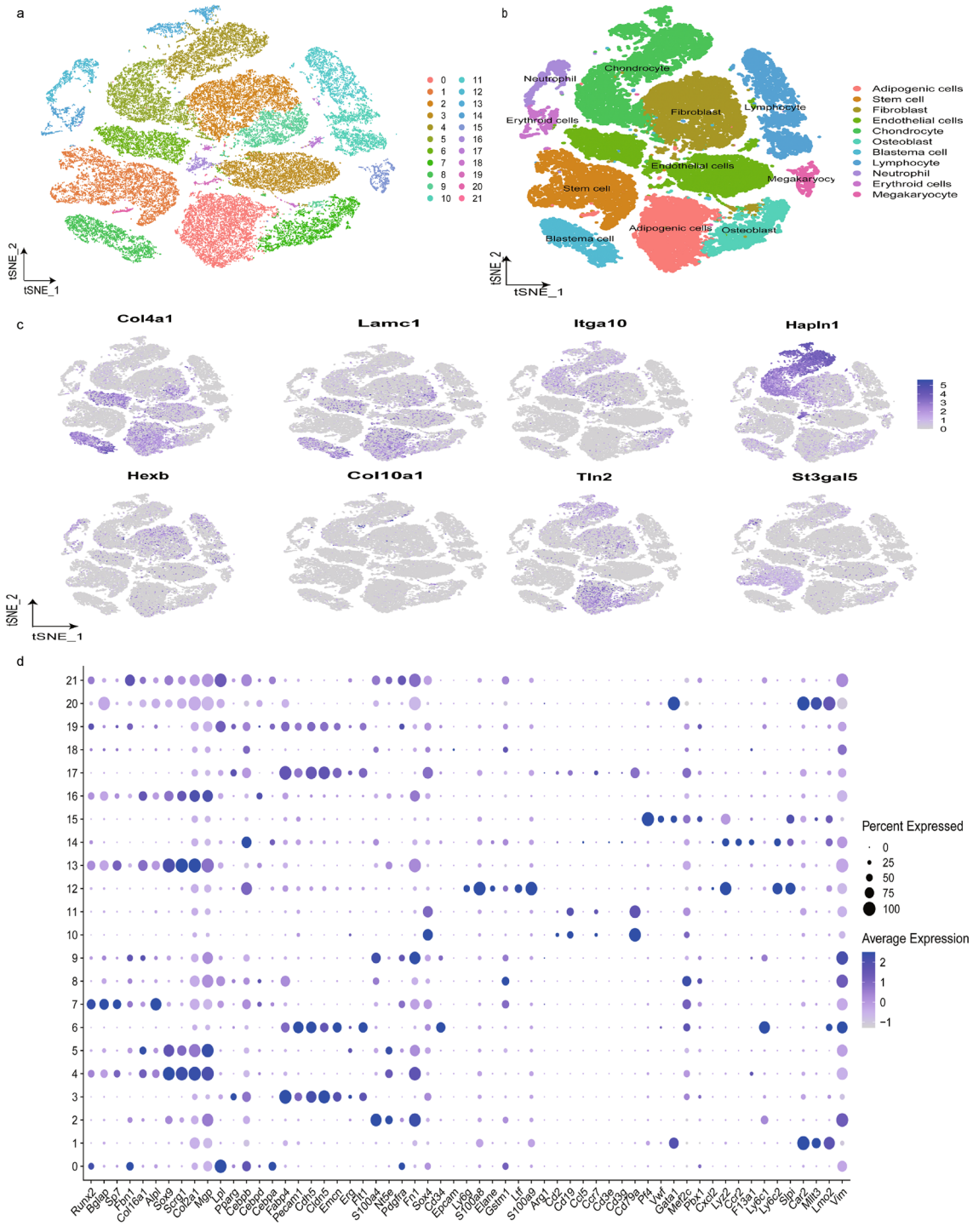

Figure 4. Subcluster identification of bone marrow-derived MSC single-cell sequencing data. (**a**) The TSNE algorithm was applied to the first 17 PCAs for dimensionality reduction, and 22 cell clusters were successfully classified; (**b**) cell clusters were manually annotated with CellMarker 2.0 according to the composition of marker genes and were successfully annotated into 11 subpopulations; (**c**) the expression levels of the target genes (Col 4a1,Lamc1,Itga10,Hapln1,Hexb,Col10a1,Tln2,St3gal5)in the subpopulations; (**d**) the marker gene bubble map. Reliability of subcluster annotation of single-cell data.

osteoblasts, and adipocytes, and based on the results of Cytotrace, Monocle2 was used to determine the direction of differentiation of the four types of cells and to determine the site of expression of the target gene.

The CellChat package was used to query the role of intercellular communication, and the ECM-Receptor database was selected for subsequent analysis based on the KEGG enrichment results. The identify OverExpressedGenes function of the CellChat package was used to identify highly expressed genes, the identify OverExpressedInteractions function was used to identify highly expressed pathways, the project Data function was

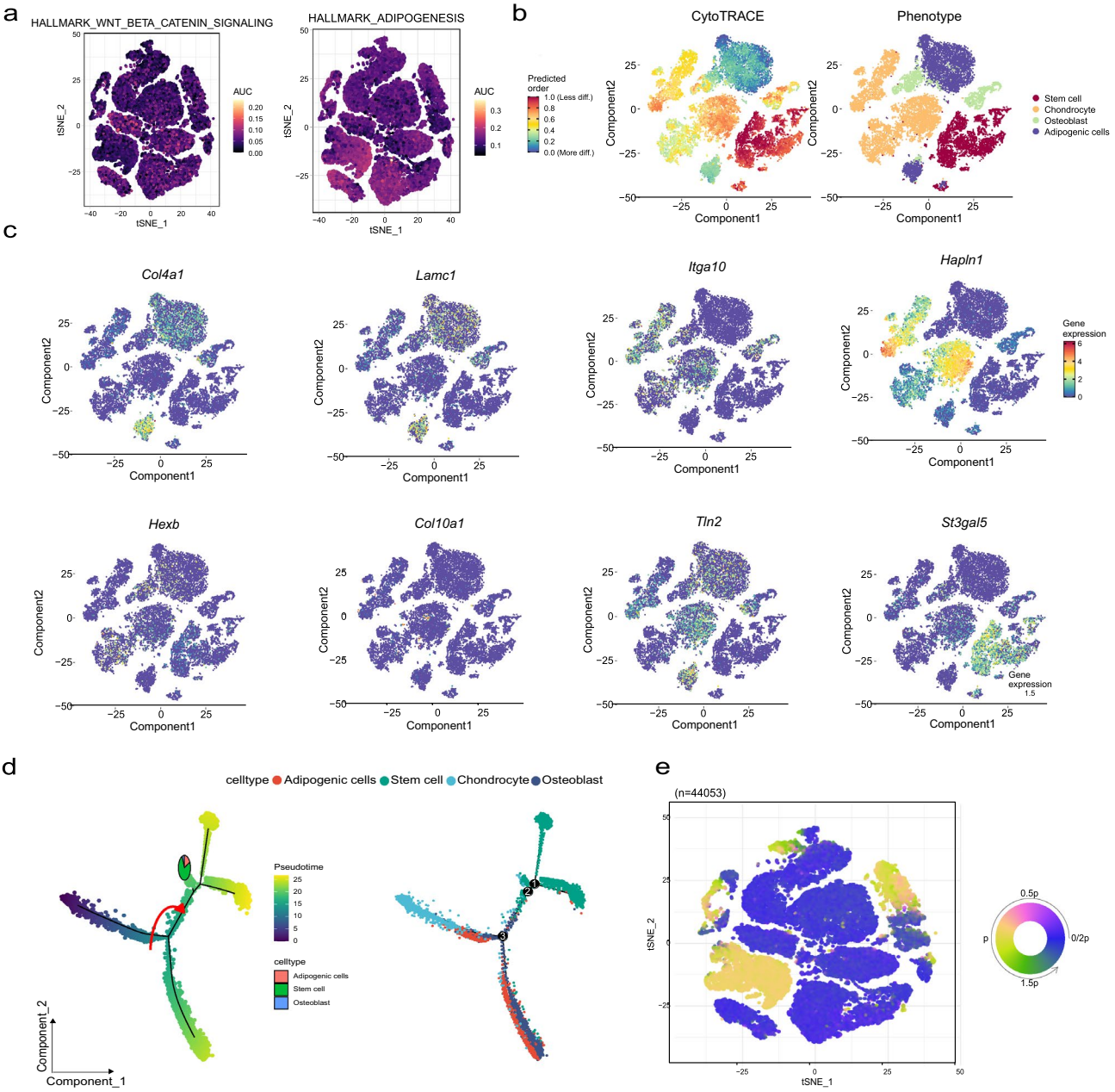

Figure 5. Proof of subgroup annotation reliability (**a**) the WNT pathway and the adult ADIPOGENESIS pathway were selected to score the cell subclusters; (**b**) the differentiation of the four classes of cells was assessed according to Cytotrace; (**c**) the expression levels of the target genes (Col4a1,Lamc1,Itga10,Hapln1,Hexb,Col10 a1,Tln2,St3gal5)according to Cytotrace; (**d**) the differentiation of the four classes of cells was assessed based on Monocle2; (**e**)the differentiation of the 11 classes of cells was assessed based on Tricycle.

used to project the relationship between the highly expressed genes and the pathways to the PPI network, the computeCommunProb function was used to calculate the probability of cell-to-cell communication, data with the minimum number of cells less than 10 were removed, the computeCommunProbPathway function was used to calculate the cell-to-cell communication at the level of signaling pathways, the aggregateNet function was used to calculate the aggregated cell-to-cell communication network, and the "LAMININ" signaling pathway was extracted.

The mechanism map was drawn via Figdraw (https://www.figdraw.com/static/index.html).

PPI network construction

The String website (https://cn.string-db.org/) analyzed protein functional interactions and selected interactions with a composite score>0.4. The RNAInter database (http://www.rnainter.org/) is a complete source of RNA interaction data for studying the relationships between mRNAs, lncRNAs, and microRNAs. The RNAInter database was used to identify miRNAs that interact with mRNAs, as well as lncRNAs that interact with miRNAs,

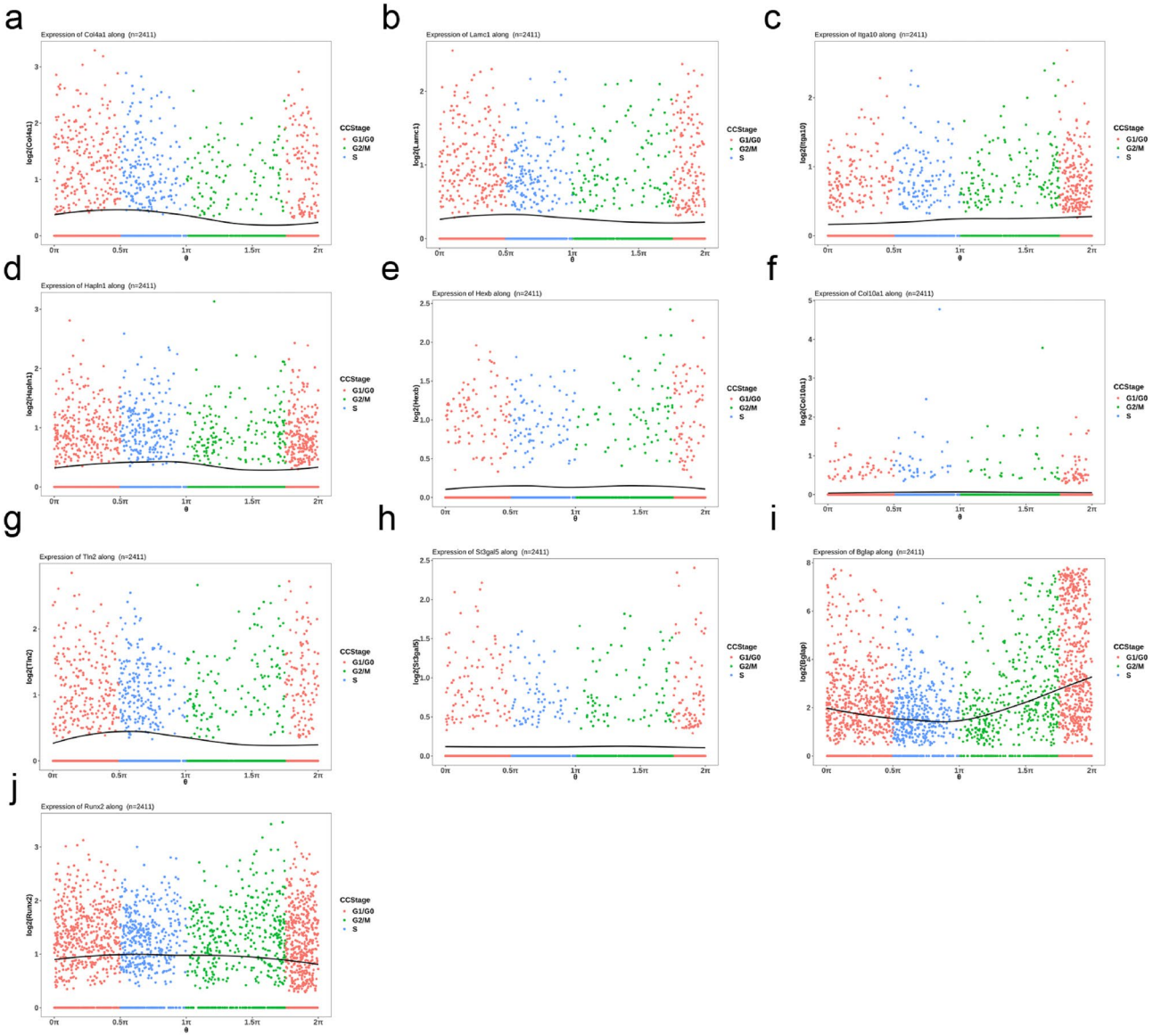

Figure 6. Expression period of target genes of Lamc1 interaction in osteoblasts (**a**) Col4a1; (**b**) Lamc1; (**c**) Itga10; (**d**) Hapln1; (**e**) Hexb; (**f**) Col10a1; (**g**) Tln2; (**h**) St3gal5;(**i**) Bglap; (**j**) Runx2.

and interactions with a score > 0.5 was selected. Cytoscape (version v3.9.1) is an open-source bioinformatics software platform for visualizing molecular interaction networks. The relationship between target genes and non-coding RNAs was plotted using Cytoscape.

Tissue distribution and gene expression identification

Protein and gene expression levels in bone marrow and adipose tissue were compared with those in the HPA database using The Human Protein Atlas (https://www.proteinatlas.org/) as a validation tool to determine whether there are differences in the expression of these genes in osteogenic and adipogenic differentiation. Expression scores in abdominal adipose tissue, omental fat pads, subcutaneous adipose tissue, tibia, synovial tissue, synovial joints, cartilage tissue, trabecular bone tissue, and bone marrow tissue were used to validate whether there are differences in the expression of these genes in osteogenic and adipogenic as well as cartilaginous differentiation using the BGEE database (https://bgee.org/). Bar graphs were drawn using GraphPad Prism 9.

Cell culture and differentiation

MC3T3-E1 cells (Procell Life, Science & Technology, China) were cultured in MEMα medium supplemented with 10% fetal bovine serum (FBS), 100 units/ml penicillin and streptomycin at 37 °C in a 5% CO_2 incubator. The medium was changed every 2–3 days and the cells were used for experiments in which the cells were grown to the logarithmic growth phase. For osteogenic differentiation, MC3T3-E1 cells were cultured in osteogenic medium supplemented with 10 mM β-glycerophosphate and 50 μg/mL L ascorbic acid osteogenic inducer. The

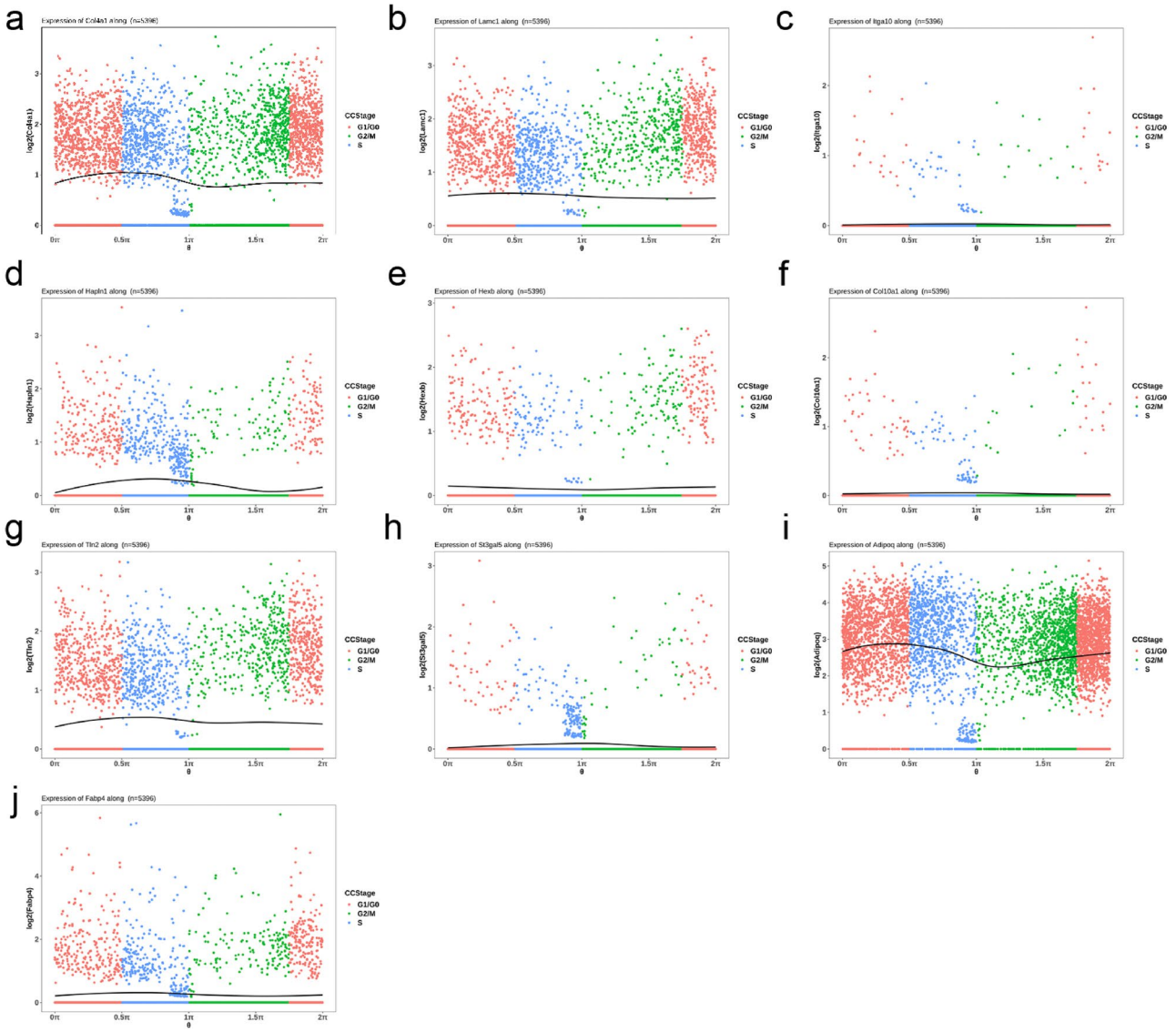

Figure 7. Expression period of target genes of Lamc1 interaction in in adipocytes (**a**) Col4a1; (**b**) Lamc1; (**c**) Itga10; (**d**) Hapln1; (**e**) Hexb; (**f**) Col10a1; (**g**) Tln2; (**h**) St3gal5;(**i**) Adipoq; (**j**) Fabp4.

cells were induced for 3, 5, or 7 days. 3T3-L1 cells (Procell Life, Science & Technology, China) were cultured in DMEM medium supplemented with 10% fetal bovine serum (FBS), 100 units/ml penicillin and streptomycin at 37 °*C* in a 5% CO_2 incubator.The medium was changed every 2-3 days, and the cells were used for experiments in which the cells were grown to the logarithmic growth phase. For adipogenic differentiation, 3T3-L1 cells were cultured in adipogenic induction medium supplemented with 0.5 μM 3-isobutyl-1-methyl xanthine , 1 μM dexamethasone and 10 μg/mL insulin adipogenic inducer for 2 days, and the medium was replaced with adipogenic maintenance medium supplemented with 10 μg/mL insulin for 2 days. The medium was finally replaced with DMEM, and the culture was continued for 2–4 days.

Alizarin red staining method and Oil Red O staining

After fixation with 80% ethanol for 30 min, cells were incubated with fresh alizarin red solution (Cyagen) for 10 min. After fixation with 4% neutral formaldehyde for 30 min, cells were incubated with saturated Oil Red O staining solution (Beyotime Biotechnology; Shanghai; China) for 10 min.

Quantitative reverse transcription PCR

Total RNA was extracted using triazole lysate lysis (Sangon Biotech; Shanghai; China), isopropanol, chloroform, and 75% ethanol solutions. Total RNA reverse transcription was induced using the HiScirpt Reverse Transcriptase kit (Novozymes Bio; Nanjing; China) The genes and primers used in the osteogenesis and adipogenesis process are listed in Table 3. Performed with a QuantStudio 5 real-time fluorescent quantitative PCR system (Applied Biosystems; Shanghai; China). Each sample was performed in triplicate. The sequences of the mRNAs were calculated according to the $\Delta\Delta C_T$ relative stacking method. mRNAs were sequenced as Table 3.

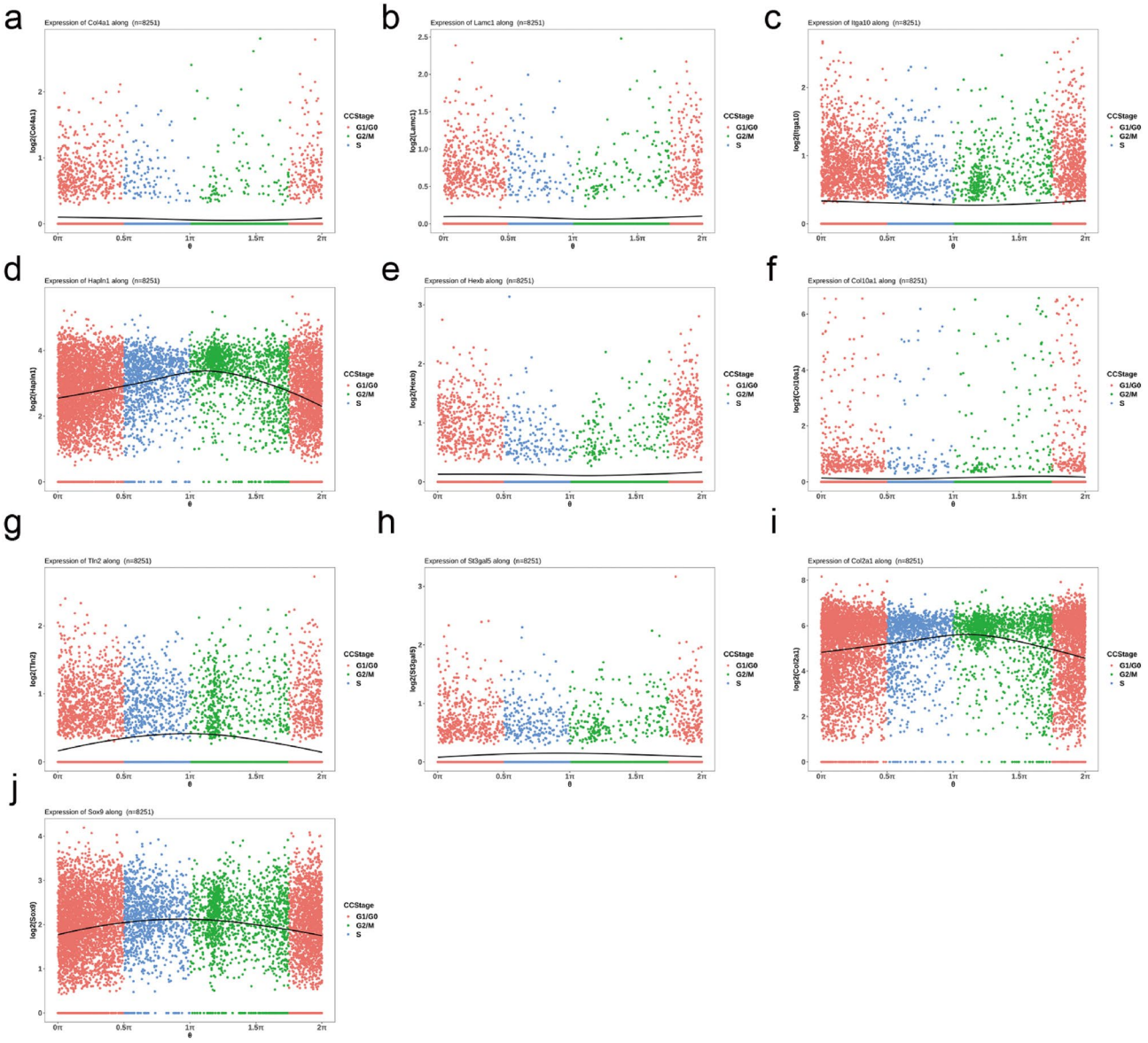

Figure 8. Expression period of target genes of Lamc1 interaction in chondrocy (**a**) Col4a1; (**b**) Lamc1; (**c**) Itga10; (**d**) Hapln1; (**e**) Hexb; (**f**) Col10a1; (**g**) Tln2; (**h**) St3gal5; (**i**) Col2a1; (**j**) Sox9.

Lamc1 siRNA interference

Lamc1 siRNA was obtained from GenePharma Corporation. siRNA was transfected into MC3T3-El cells using the gp transfection mate (GenePharma Corporation) according to the manufacturer's instructions. 24 h later, induction was initiated, and cells were collected 3–7 days later for alizarin red staining, and real-time quantitative RT PCR analysis. The siRNA was transfected into 3T3-L1 cells using gp transfection mate (GenePharma Corporation) according to the manufacturer's instructions. After 90% confluence, induction was initiated, and the cells were collected 4–8 days later for oil red o staining, and real-time quantitative qPCR analysis experiments. The sequence of the siRNA was as follows. NC:5′-UUCUCCGAACGUGUCACGUTT-3′ and 5′-ACG UGACACGUUCGGAGAATT-3′; Lamc1-siRNA: 5′-GCCGUAAUCUCAGACAGUUTT-3′ and 5′- AACUGU CUGAGAUUACGGCTT-3′.

Molecular docking analysis

The Hdock website (http://hdock.phys.hust.edu.cn/) was used to perform simulated docking studies of Laminin-111 (Entry ID:5mc9)with DAG1 (Entry ID: 5llk) or CD44 (Entry ID:4pz3), the PymoL software (version v3.0.0) was used to perform pre-docking treatments (water molecules from the structure and co-crystallized ligands were removed, H atoms were added) and Pymol was used for the visual presentation of the docking complexes, with the results with the highest docking scores being selected.

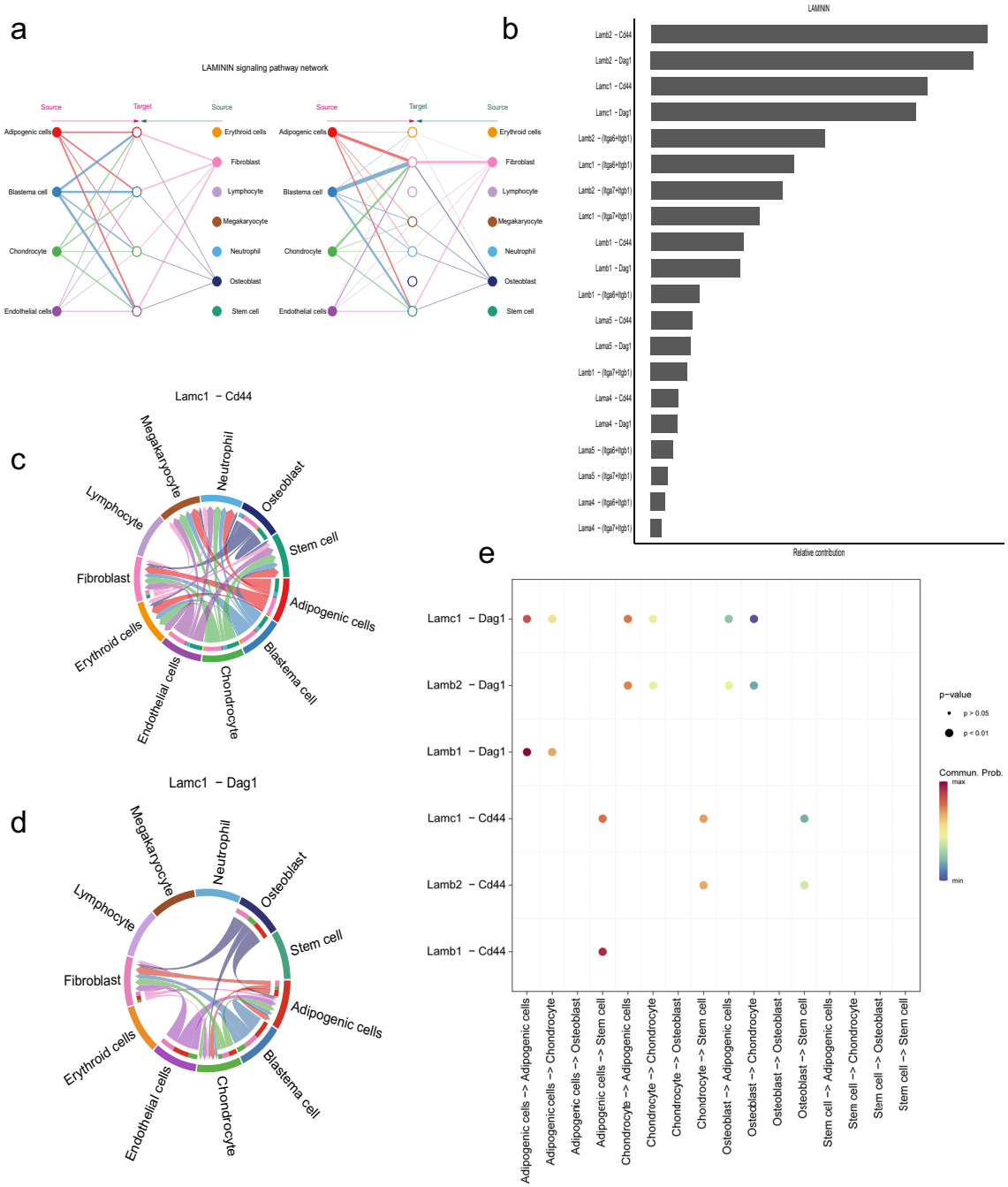

Figure 9. The molecular mechanism of Lamc1 interaction (**a**) hierarchical plot of cellular communication; (**b**) the most important ligand-receptor interactions in the laminin pathway (top 20); (**c**) LAMC1-Dag1 interaction chord diagram; (**d**) LAMC1-CD44 interaction chord diagram; (**e**) Demonstrate the specific ligand–receptor interaction mechanisms of stem cells, osteoblasts, and adipogenic and chondrogenic cells in the Laminin pathway.

Discussion

To investigate the molecular mechanisms of the multidirectional differentiation of BMSCs, especially osteogenesis, adipogenesis and chondrogenesis, BMSCs exhibited significant cellular heterogeneity, and an integrated analysis of the multiscale transcriptome was performed in the present study. These DEGs were analyzed by bulk RNA-seq and scRNA-seq, and it was found that the late stage of differentiation was the most significant in terms of interactions with the ECM receptor. It is well known that the ECM enhances cell recruitment through cell surface receptors, which determine cellular interactions with the ECM and trigger specific cellular functions such as adhesion, migration, proliferation, and differentiation[30]. Several studies have reported the critical role of the matrix in regulating the differentiation of MSCs toward the bone or adipose lineage[30,31].Recent studies have shown that stem cells can mechanically sense the hardness of their microenvironment, and the direction

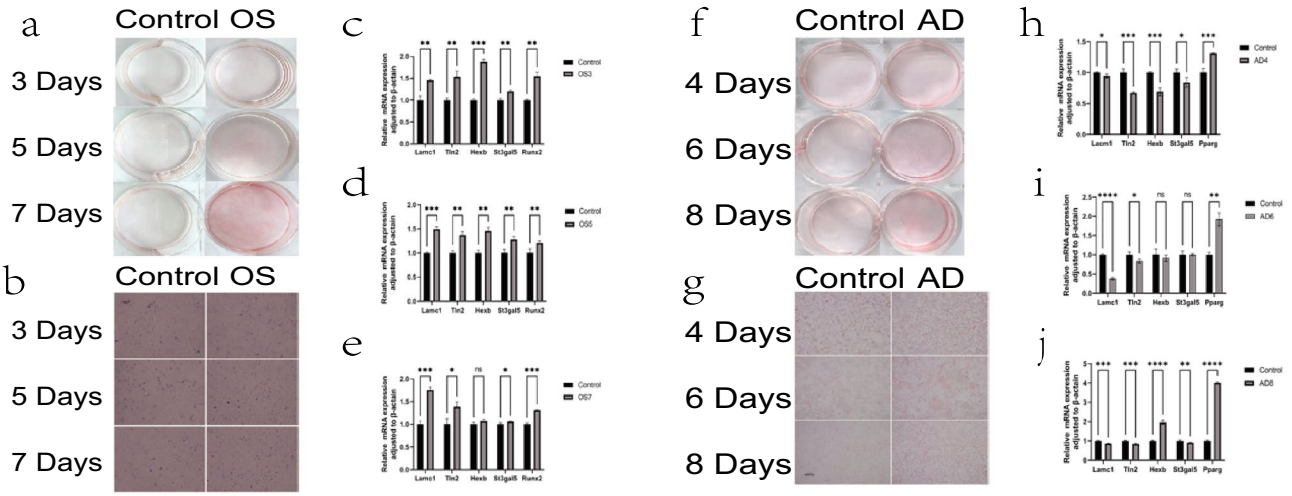

Figure 10. Results of target gene expression experiments. (**a**) Alizarin red staining of osteoblasts induced for 3, 5 and 7 days; (**b**) capture images with camera,100× microscope,scale bar = 500 μm; qPCR results of target gene expression in osteoblasts: (**c**) 3 days; (**d**) 5 days; (**e**) 7 days. (**f**) Oil Red O staining of adipocytes induced for 4, 6 and 8 days; (**g**) capture images with camera, 100× microscope, scale bar = 500 μm; qPCR results of target gene expression in adipocyte: (**h**) 4 days; (**i**) 6 days; (**j**) 8 days.

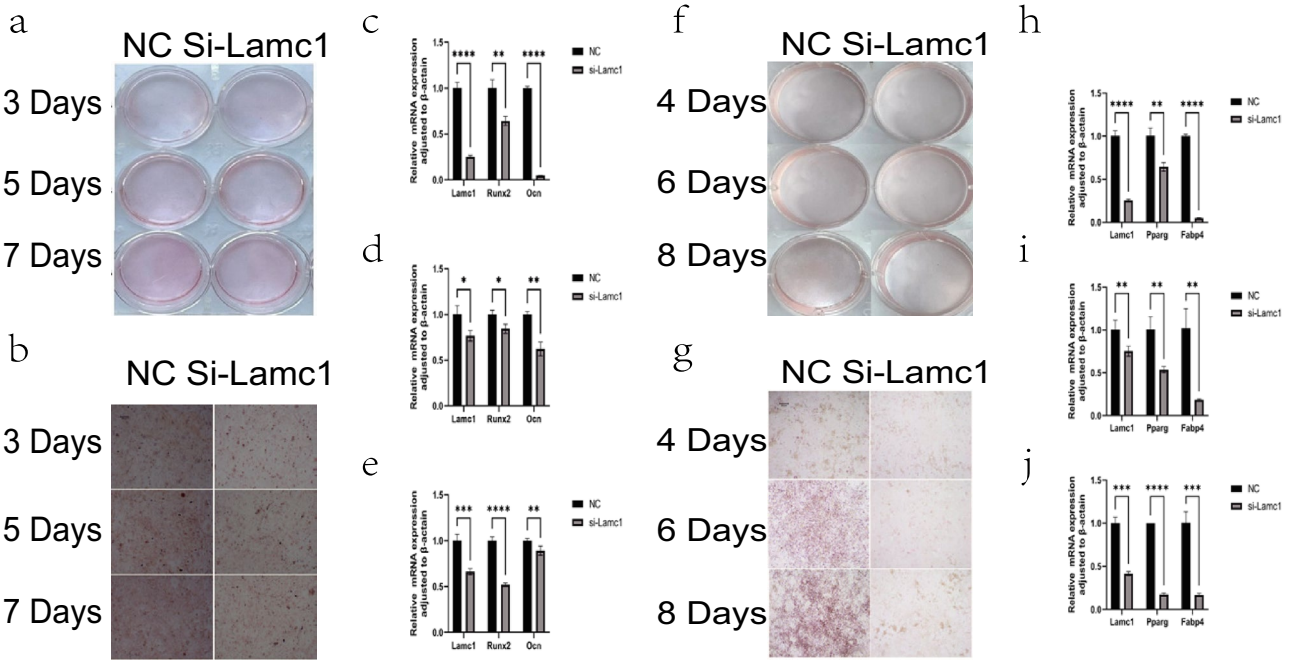

Figure 11. Results of target gene expression experiments after knockdown of Lamc1. (**a**) Alizarin red staining of osteoblasts induced for 3, 5 and 7 daysafter knockdown of Lamc1; (**b**) capture images with camera, 100× microscope,scale bar = 500 μm; qPCR results of target gene expression after knockdown of Lamc1 in osteoblasts: (**c**) 3 days; (**d**) 5 days; (**e**) 7 days. (**f**) Oil Red O staining of adipocytes induced for 4, 6 and 8 days after knockdown of Lamc1; (**g**) capture images with camera, 100 × microscope, scale bar = 500 μm; qPCR results of target gene expression after knockdown of Lamc1 in adipocyte: (**h**) 4 days; (**i**) 6 days; (**j**) 8 days.

of differentiation of MSCs may change with changes in the matrix composition[32,33]. For example, the extracellular matrix supplemented with glucan sulfate promotes the osteogenic differentiation of mesenchymal stem cells[34], and type I collagen inhibits adipogenesis and differentiation by activating yes-associated proteins[35]. The latest research by Yangzi Jiang et al. showed that ECM produced by adult stem cells from different tissues has different cartilage induction abilities[36]. Osteoblasts are the main bone-forming cells, and they produce extracellular proteins that constitute the major components of bone. During bone formation, BMSCs differentiate into osteoblasts, which produce bone by synthesizing an extracellular matrix composed of various proteins. The initial deposition of the extracellular matrix is called the osteoid, which is then mineralized into bone tissue by the accumulation of hydroxyapatite ($Ca_10(PO_4)_6(OH)_2$) as calcium phosphate[37]. As osteoblasts mature, they

DataSet	Samples	Organism	Type of cell	Differentiation time	Group	DOI
GSE36923	GSM906367, GSM906368, GSM906369.	Homo sapiens	BMSCs	0 Day	Control	10.1016/j.biocel.2013.11.010
	GSM906370, GSM906371, GSM906372.			15 Days	Adipogenic	
GSE44303	GSM1082817, GSM1082818, GSM1082819.	Homo sapiens	BMSCs	0 Day	Control	10.1093/nar/gku567
	GSM1082844, GSM1082845, GSM1082846.			14 Days	Adipogenic	
GSE109503	GSM2944707, GSM2944708, GSM2944709.	Homo sapiens	BMSCs	0 Day	Control	10.1096/fj.201800534R
	GSM1082844, GSM1082845, GSM1082846.			14 Days	Chondrocyte	
GSE140861	GSM4188963, GSM4188970.	Homo sapiens	BMSCs	0 Day	Control	10.1089/ten.TEA.2016.0559
	GSM4188967, GSM4188974.			14 Days	Chondrocyte	
GSE28205	GSM698427, GSM698433, GSM698439.	Homo sapiens	BMSCs	0 Day	Control	10.1002/jbmr.1578
	GSM698429, GSM698431, GSM698436.			14 Days	Osteoblast	
GSE37558	GSM921574, GSM921575, GSM921576, GSM921578.	Homo sapiens	BMSCs	0 Day	Control	10.1186/1471-2164-15-965
	GSM921584, GSM921585, GSM921586.			12 Days	Osteoblast	
GSE128423	GSM3674224, GSM3674225, GSM3674226, GSM3674227, GSM3674228, GSM3674229.	Mus musculus	BMSCs	Undifferentiation	–	10.1016/j.cell.2019.04.040
GSE156635	GSM4735397, GSM4735398.	Mus musculus	BMSCs	Undifferentiation	–	10.1016/j.celrep.2021.109352

Table 2. Summary information on gene expression profiling datasets.

Gene	Forward primers	Reverse primers
Lamc1	TGCCGGAGTTTGTTAATGCC	TGGTTGTTGTAGTCGGTCAGG
Tln2	AGGAAAGGGATTTGGCTAGAAGC	CCAACATTCGGATTTTCTGAGGC
Hexb	CTGGTGTCGCTAGTGTCGC	CAGGGCCATGATGTCTCTTGT
St3gal5	AAAAGAATGCACTATGTGGACCC	ATAGCCGTCTTCGCGTACCT
Runx2	CGGTCTCCTTCCAGGATGGT	GCTTCCGTCAGCGTCAACA
Ocn	GAACAGACAAGTCCCACACAGC	TCAGCAGAGTGAGCAGAAAGAT
Pparγ	GGAAGACCACTCGCATTCCTT	GTAATCAGCAACCATTGGGTCA
Fabp4	ATCAGCGTAAATGGGGATTTGG	GTCTGCGGTGATTTCATCGAA
β-actin	GTGACGTTGACATCCGTAAAGA	GCCGGACTCATCGTACTCC

Table 3. qPCR primer sequences.

transform into osteocytes, and revealing the detailed mechanisms that regulate the later stages of osteoblast differentiation and function is important for clinical applications[38]. However, studies on the mechanisms underlying the differentiation of bone marrow-derived MSCs in the late stages of differentiation still need to be performed. We therefore selected an mRNA microarray dataset at the end of differentiation to identify genes that showed significant heterogeneity in the differentiation of BMSCs into adipocytes, osteoblasts, and chondrocytes. lamc1 tended to increase osteoblastic differentiation and decrease adipocytes, and Col4a1 had the opposite effect on differentiation. Highly expressed Lamc1 and Col4a1 play key roles in the protein interaction network, and their

interactions with the key molecules involved in osteogenic, adipogenic, and chondrogenic differentiation, H19, XIST, NEAT1, and MALAT1, have been identified. According to our results, Hui-jian Chen et al. reported that Lama4 and Col4a1 are expressed in white adipose tissue at different sites and are upregulated during adipocyte differentiation[39]. Interestingly, the mRNA expression of Col4a1 was significantly increased after adipogenic induction of MSCs in a recent study, which is consistent with our expectations[40]. More importantly, laminin in the cell matrix contains three subunits: α , β, and γ. Lamc1 is the most commonly used γ chain and is present in most laminin molecules[41]. During the process of osteogenesis, Laminin activates downstream signaling pathways such as Rho GTPase and MAPK by interacting with Integrin, which in turn regulates the processes of cellular bone morphogenesis and bone matrix deposition, and participates in the directional differentiation of stem cells to osteoblasts[42,43].Lamc1 is present in LN-111 and LN-511, it has been shown to promote osteogenic differentiation by binding to integrins[41],which are key factors for the development of osteoblasts. The HPA database, Bgee database, and single-cell transcriptome data analysis revealed that Lamc1 expression was significantly greater in adipocytes than in osteoblasts, but Lamc1 tended to promote bone formation and inhibit adipogenic, and this tendency became more obvious with increasing induction time. Further studies showed that after Lamc1 knockdown, the expression of osteogenic and adipogenic markers was significantly decreased, and differentiation was inhibited. It is therefore reasonable to assume that Lamc1 plays an important role in regulating the balance of bone adipogenesis[44].

The distribution of target genes in bone marrow-derived MSCs, the cell cycle, and ligand–receptor interactions were determined by single-cell transcriptome analysis. Among these genes, Lamc1, which is expressed mainly during the G2/M phase in adipogenic cells and may affect intracellular signaling through interactions with Dag1, was used as a focus for determining the balance between osteogenic and adipogenic differentiation. Dag1 (also known as α-glycoprotein) is involved in the adhesion between the extracellular matrix and cells, helps to maintain cell aggregation and structural stability, and participates in the assembly process of laminin and the basement membrane[45]. Recent studies have shown that Dag1 plays a role in cartilage formation and osteoblast differentiation in vivo[46,47].Another finding is that the interaction of Dag1 with laminin has been reported[48].To prove our prediction, molecular docking experiments were performed on laminin and Dag1. The experimental results showed that laminin and Dag1 formed a total of 11 hydrogen bonds (Fig. 12a). Our data support the conclusion that the interaction of Dag1 and Lamc1 may influence the balance between the adipogenic and osteogenic differentiation of MSCs through cell adhesion, signaling, and gene regulation (Fig. 12c). Similarly, a total of four hydrogen bonds were formed after molecular docking experiments were performed on laminin and CD44, initially validating the interaction between Lamc1 and CD44 (Fig. 12b).

In conclusion, this study aimed to identify DEGs that may be involved in osteogenic differentiation, adipogenic differentiation, and the onset and progression of chondrogenic differentiation of bone marrow mesenchymal stem cells (BMSCs). A total of eight hub genes were identified, four of which were discovered and proposed for the first time in this study. Although these findings are preliminary, they suggest the existence of previously unknown regulatory relationships governing the differentiation process of BMSCs. Unfortunately, our experiments did not reveal new regulatory relationships between chondrogenesis and adipogenesis or osteogenesis, which may be related to our choice of a more conservative data merging approach.However, this conservative strategy ensured the accuracy of bioinformatic predictions. Despite these limitations, the identified hub genes and their potential interactions provide valuable insights and lay the foundation for further investigation into the molecular mechanisms underlying the multi-lineage differentiation of BMSCs.

Conclusion

This study aimed to identify the key biological processes involved in the late stages of differentiation of BMSCs. The following conclusions were demonstrated: eight target genes were identified in the context of trilineage differentiation antagonism, which is concentrated in the extracellular matrix and is associated with ECM-receptor interactions.Notably, Lamc1 expression was higher in adipose tissue than in bone tissue. Furthermore, Lamc1 exhibited maximal expression during the mitotic phase of the cell cycle. Bioinformatic analysis suggested that Lamc1 interacts with CD44 and may influence the differentiation of stem cells towards osteoblastic, chondrogenic, or adipogenic lineages. Additionally, the interaction between Lamc1 and Dag1 may affect the balance of trilineage differentiation in BMSCs. Experimental validation confirmed that Lamc1 was upregulated during osteogenic differentiation and downregulated during adipogenic differentiation, indicating its essential role in regulating the differentiation process.

Data availibility

The datasets covered in this reasearch are all publicly available transcriptomic data from the Gene Expression Omnibus (GEO). Ullah M, Sittinger M, Ringe J. Transdifferentiation of adipogenically differentiated cells into

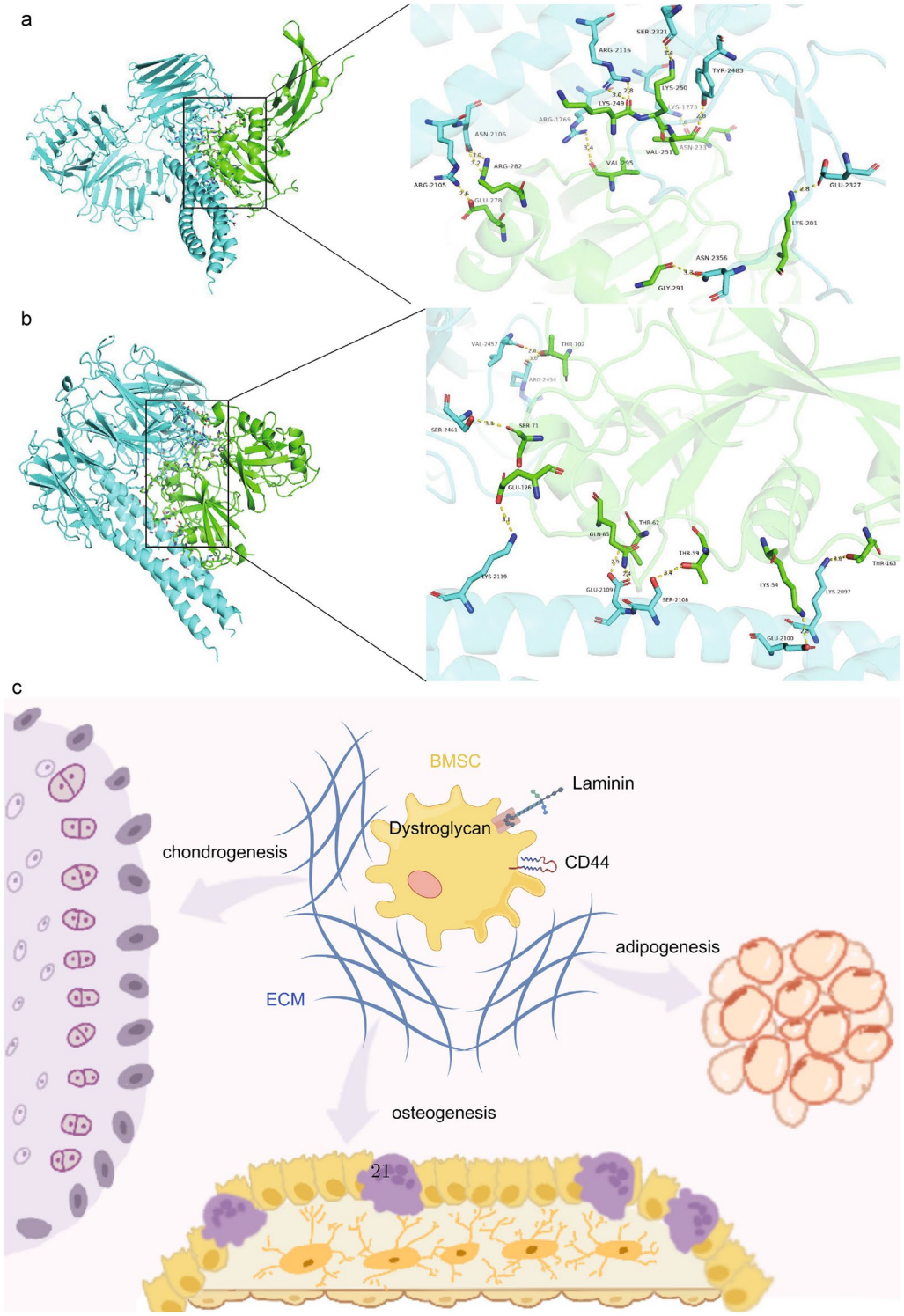

Figure 12. Molecular docking and mechanism maps (**a**) Results of molecular docking of laminin to DAG1; (**b**) Results of molecular docking of laminin to CD44; (**c**) mechanism maps.

osteogenically or chondrogenically differentiated cells: phenotype switching via dedifferentiation. Int J Biochem Cell Biol. 2014 Jan;46:124-37. doi: 10.1016/j.biocel.2013.11.010. Epub 2013 Nov 22. GSE36923. Tomaru Y, Hasegawa R, Suzuki T, Sato T, Kubosaki A, Suzuki M, Kawaji H, Forrest AR, Hayashizaki Y; FANTOM Consortium; Shin JW, Suzuki H. A transient disruption of fibroblastic transcriptional regulatory network facilitates trans-differentiation. Nucleic Acids Res. 2014 Aug;42(14):8905-13. doi: 10.1093/nar/gku567. Epub 2014 Jul 10. GSE44303. Huynh NPT, Zhang B, Guilak F. High-depth transcriptomic profiling reveals the temporal gene

signature of human mesenchymal stem cells during chondrogenesis. FASEB J. 2019 Jan;33(1):358-372. doi: 10.1096/fj.201800534R. Epub 2018 Jul 9. GSE109503. Somoza RA, Correa D, Labat I, Sternberg H, Forrest ME, Khalil AM, West MD, Tesar P, Caplan AI. Transcriptome-Wide Analyses of Human Neonatal Articular Cartilage and Human Mesenchymal Stem Cell-Derived Cartilage Provide a New Molecular Target for Evaluating Engineered Cartilage. Tissue Eng Part A. 2018 Feb;24(3-4):335-350. doi: 10.1089/ten.TEA.2016.0559. Epub 2017 Jul 28.GSE140861. Dani N, Olivero M, Mareschi K, van Duist MM, Miretti S, Cuvertino S, Patané S, Calogero R, Ferracini R, Scotlandi K, Fagioli F, Di Renzo MF. The MET oncogene transforms human primary bone-derived cells into osteosarcomas by targeting committed osteo-progenitors. J Bone Miner Res. 2012 Jun;27(6):1322-34. doi: 10.1002/jbmr.1578. GSE28205. Alves RD, Eijken M, van de Peppel J, van Leeuwen JP. Calcifying vascular smooth muscle cells and osteoblasts: independent cell types exhibiting extracellular matrix and biomineralization-related mimicries. BMC Genomics. 2014 Nov 7;15(1):965. doi: 10.1186/1471-2164-15-965. GSE37558. Baryawno N, Przybylski D, Kowalczyk MS, Kfoury Y, Severe N, Gustafsson K, Kokkaliaris KD, Mercier F, Tabaka M, Hofree M, Dionne D, Papazian A, Lee D, Ashenberg O, Subramanian A, Vaishnav ED, Rozenblatt-Rosen O, Regev A, Scadden DT. A Cellular Taxonomy of the Bone Marrow Stroma in Homeostasis and Leukemia. Cell. 2019 Jun 13;177(7):1915-1932.e16. doi: 10.1016/j.cell.2019.04.040. Epub 2019 May 23. GSE128423. Sivaraj KK, Jeong HW, Dharmalingam B, Zeuschner D, Adams S, Potente M, Adams RH. Regional specialization and fate specification of bone stromal cells in skeletal development. Cell Rep. 2021 Jul 13;36(2):109352. doi: 10.1016/j.celrep.2021.109352.GSE156635.

Received: 15 May 2024; Accepted: 7 August 2024
Published online: 23 August 2024

References

1. Johnson, J. *et al.* From mesenchymal stromal cells to engineered extracellular vesicles: A new therapeutic paradigm. *Front. Cell Dev. Biol.* **9**, 705676 (2021).
2. Chen, Q. *et al.* Fate decision of mesenchymal stem cells: Adipocytes or osteoblasts?. *Cell Death Differ.* **23**(7), 1128–1139 (2016).
3. Jain, M. *et al.* Amniotic fluid mesenchymal stromal cells derived from fetuses with isolated cardiac defects exhibit decreased proliferation and cardiomyogenic potential. *Biology* **12**(4), 552 (2023).
4. Biswas, A. *et al.* Human placenta/umbilical cord derivatives in regenerative medicine—Prospects and challenges. *Biomater. Sci.* **11**(14), 4789–4821 (2023).
5. Liebig, B. E. *et al.* The platelet-rich plasma and mesenchymal stem cell milieu: A review of therapeutic effects on bone healing. *J. Orthop. Res.* **38**(12), 2539–2550 (2020).
6. Jiang, Y., Zhang, P., Zhang, X., *et al*. Advances in mesenchymal stem cell transplantation for the treatment of osteoporosis. *Cell Prolif.* **54**(1), (2021).
7. Mohamed-Ahmed, S. *et al.* Adipose-derived and bone marrow mesenchymal stem cells: A donor-matched comparison[J]. *Stem Cell Res. Therapy* **9**(1), 168 (2018).
8. Liu, D. D. *et al.* RUNX2 regulates osteoblast differentiation via the BMP4 signaling pathway. *J. Dent. Res.* **101**(10), 1227–1237 (2022).
9. Komori, T. Functions of osteocalcin in bone, pancreas, testis, and muscle. *Int. J. Mol. Sci.* **21**(20), 7513 (2020).
10. Fisher, L. A. B. & Schöck, F. The unexpected versatility of ALP/Enigma family proteins. *Front. Cell Dev. Biol.* **10**, 963608 (2022).
11. Kriegel, A. *et al.* Bone sialoprotein immobilized in collagen type I enhances bone regeneration in vitro and in vivo. *Int. J. Bioprint.* **8**(3), 591 (2022).
12. Wei, J. *et al.* Glucose uptake and Runx2 synergize to orchestrate osteoblast differentiation and bone formation. *Cell* **161**(7), 1576–1591 (2015).
13. Neve, A., Corrado, A. & Cantatore, F. P. Osteocalcin: Skeletal and extra-skeletal effects. *J. Cell. Physiol.* **228**(6), 1149–1153 (2013).
14. Tóth, F. *et al.* Effect of inducible bone morphogenetic protein 2 expression on the osteogenic differentiation of dental pulp stem cells in vitro. *Bone* **132**, 115214 (2020).
15. Cheng, H. *et al.* Bone morphogenetic protein 4 rescues the bone regenerative potential of old muscle-derived stem cells via regulation of cell cycle inhibitors. *Stem Cell Res. Ther.* **13**(1), 385 (2022).
16. Bharadwaz, A. & Jayasuriya, A. C. Osteogenic differentiation cues of the bone morphogenetic protein-9 (BMP-9) and its recent advances in bone tissue regeneration[J]. *Mater. Sci. Eng. C Mater. Biol. Appl.* **120**, 111748 (2021).
17. Deng, L. *et al.* MFN2 knockdown promotes osteogenic differentiation of iPSC-MSCs through aerobic glycolysis mediated by the Wnt/β-catenin signaling pathway[J]. *Stem Cell Res. Ther.* **13**(1), 162 (2022).
18. Cao, Y. *et al.* PPARγ as a potential target for adipogenesis induced by fine particulate matter in 3T3-L1 preadipocytes. *Environ. Sci. Technol.* **57**(20), 7684–7697 (2023).
19. Liu, C. *et al.* CHD7 regulates bone-fat balance by suppressing PPAR-γ signaling. *Nat. Commun.* **13**(1), 1989 (2022).
20. Liu, Z.-Z. *et al.* Autophagy receptor OPTN (optineurin) regulates mesenchymal stem cell fate and bone-fat balance during aging by clearing FABP3. *Autophagy* **17**(10), 2766–2782 (2021).
21. Benayahu, D., Wiesenfeld, Y. & Sapir-Koren, R. How is mechanobiology involved in mesenchymal stem cell differentiation toward the osteoblastic or adipogenic fate?. *J. Cell. Physiol.* **234**(8), 12133–12141 (2019).
22. Levi, N. *et al.* The ECM path of senescence in aging: Components and modifiers. *FEBS J.* **287**(13), 2636–2646 (2020).
23. Yanli, Z. *et al.* MY-1-loaded nano-hydroxyapatite accelerated bone regeneration by increasing type III collagen deposition in early-stage ECM via a Hsp47-dependent mechanism. *Adv. Healthc. Mater.* **12**(20), e2300332 (2023).
24. Wang, Y. *et al.* Impact of fibronectin knockout on proliferation and differentiation of human infrapatellar fat pad-derived stem cells. *Front. Bioeng. Biotechnol.* **7**, 321 (2019).
25. Xiong, X. *et al.* Extracellular matrix derived from human urine-derived stem cells enhances the expansion, adhesion, spreading, and differentiation of human periodontal ligament stem cells. *Stem Cell Res. Ther.* **10**(1), 396 (2019).
26. Cai, R. *et al.* Matrices secreted during simultaneous osteogenesis and adipogenesis of mesenchymal stem cells affect stem cells differentiation. *Acta Biomater.* **35**, 185–193 (2016).
27. Zhang, D. *et al.* CircRNA-vgll3 promotes osteogenic differentiation of adipose-derived mesenchymal stem cells via modulating miRNA-dependent integrin α5 expression. *Cell Death Differ.* **28**(1), 283–302 (2021).
28. Morandi, E. M. *et al.* ITGAV and ITGA5 diversely regulate proliferation and adipogenic differentiation of human adipose derived stem cells. *Sci. Rep.* **6**, 28889 (2016).
29. Zhu, J., Li, J., Yao, T., *et al.* Analysis of the role of irisin receptor signaling in regulating osteogenic/adipogenic differentiation of bone marrow mesenchymal stem cells. *Biotechnol. Genet. Eng. Rev.* 1–24 (2023).

30. Hu, M., Ling, Z. & Ren, X. Extracellular matrix dynamics: Tracking in biological systems and their implications. *J. Biol. Eng.* **16**, 13 (2022).
31. Schlesinger, P. H. *et al.* Cellular and extracellular matrix of bone, with principles of synthesis and dependency of mineral deposition on cell membrane transport. *Am. J. Physiol. Cell Physiol.* **318**(1), C111–C124 (2020).
32. El-Rashidy, A. A. *et al.* Effect of polymeric matrix stiffness on osteogenic differentiation of mesenchymal stem/progenitor cells: Concise review. *Polymers* **13**(17), 2950 (2021).
33. Chen, Y. *et al.* ECM scaffolds mimicking extracellular matrices of endochondral ossification for the regulation of mesenchymal stem cell differentiation. *Acta Biomater.* **114**, 158–169 (2020).
34. Wan, H.-Y. *et al.* Dextran sulfate-amplified extracellular matrix deposition promotes osteogenic differentiation of mesenchymal stem cells. *Acta Biomater.* **140**, 163–177 (2022).
35. Liu, X. *et al.* Type I collagen inhibits adipogenic differentiation via YAP activation in vitro. *J. Cell. Physiol.* **235**(2), 1821–1837 (2020).
36. Jiang, Y. & Tuan, R. S. Bioactivity of human adult stem cells and functional relevance of stem cell-derived extracellular matrix in chondrogenesis. *Stem Cell Res. Ther.* **14**(1), 160 (2023).
37. Lin, X. *et al.* The bone extracellular matrix in bone formation and regeneration. *Front. Pharmacol.* **11**, 757 (2020).
38. O'Doherty, M. *et al.* Improving the intercellular uptake and osteogenic potency of calcium phosphate via nanocomplexation with the RALA peptide. *Nanomaterials (Basel, Switzerland)* **10**(12), 2442 (2020).
39. Chen, H. Adipose extracellular matrix deposition is an indicator of obesity and metabolic disorders. *J. Nutr. Biochem.* **111**, 109159 (2023).
40. Ullah, M., Sittinger, M. & Ringe, J. Extracellular matrix of adipogenically differentiated mesenchymal stem cells reveals a network of collagen filaments, mostly interwoven by hexagonal structural units. *Matrix Biol.* **32**(7–8), 452–465 (2013).
41. Chen, C., Jiang, Z. & Yang, G. Laminins in osteogenic differentiation and pluripotency maintenance. *Differentiation* **114**, 13–19 (2020).
42. Yap, L. Laminins in cellular differentiation. *Trends Cell Biol.* **29**(12), 987–1000 (2019).
43. Sun, M. Extracellular matrix stiffness controls osteogenic differentiation of mesenchymal stem cells mediated by integrin α5. *Stem Cell Res. Ther.* **9**(1), 52 (2018).
44. Yang, Y. *et al.* Mesenchymal Stem cell-derived extracellular matrix enhances chondrogenic phenotype of and cartilage formation by encapsulated chondrocytes in vitro and in vivo. *Acta Biomater.* **69**, 71–82 (2019).
45. Henry, M. D. *et al.* Distinct roles for dystroglycan, β1 integrin and perlecan in cell surface laminin organization. *J. Cell Sci.* **114**(Pt 6), 1137–1144 (2001).
46. Souza, A. T. P. *et al.* The extracellular matrix protein Agrin is expressed by osteoblasts and contributes to their differentiation. *Cell Tissue Res.* **386**(2), 335–347 (2021).
47. Eldridge, S. *et al.* Agrin mediates chondrocyte homeostasis and requires both LRP4 and α-dystroglycan to enhance cartilage formation in vitro and in vivo. *Ann. Rheum. Dis.* **75**(6), 1228–1235 (2016).
48. in, S. H., Kim, S. K. & Lee, S. B. M. leprae interacts with the human epidermal keratinocytes, neonatal (HEKn) via the binding of laminin-5 with α-dystroglycan, integrin-β1, or -β4[J]. *PLoS Negl. Trop. Dis.* **13**(6), e0007339 (2019).

Author contributions

L.Z. and S.L. wrote the main manuscript text and Y.P. typesetted and checked the manuscripts. J.Z. led and supervised the planning and execution of the experiments. All authors reviewed the manuscript.

Funding

This research was supported by the National Natural Science Foundation of China (Grant numbers 81960171 and 82360167) and Guizhou Provincial Science and Technology Program (Guizhou Science and Technology Foundation-ZK[2022] General 620).

Competing interests

The authors declare no competing interests.

Additional information

Supplementary Information The online version contains supplementary material available at https://doi.org/10.1038/s41598-024-69629-4.

Correspondence and requests for materials should be addressed to J.Z.